Chinese Physics Letters **42**, 067304 (2025) **Express Letter**

Evidence for Mobile Gapless Spinons in a Honeycomb Lattice

Chengpeng Tu[1†], Dongzhe Dai[1†], Xu Zhang[1], Chengcheng Zhao[1], Xiaobo Jin[1], Bin Gao[2], Tong Chen[2], Pengcheng Dai[2], and Shiyan Li[1,3,4,5*]

[1] *State Key Laboratory of Surface Physics, and Department of Physics, Fudan University, Shanghai 200438, China*
[2] *Department of Physics & Astronomy and Smalley-Curl Institute, Rice University, Houston, Texas 77005, USA*
[3] *Shanghai Research Center for Quantum Sciences, Shanghai 201315, China*
[4] *Shanghai Branch, Hefei National Laboratory, Shanghai 201315, China*
[5] *Collaborative Innovation Center of Advanced Microstructures, Nanjing 210093, China*

(Received 14 May 2025; accepted manuscript online 29 May 2025)

One important issue in current condensed matter physics is the search of quantum spin liquid (QSL), an exotic magnetic state with strongly-fluctuating and highly-entangled spins down to zero temperature without static order. However, there is no consensus on the existence of a QSL state in any real material so far, due to inevitable disorder and intricate competing exchange interactions on frustrated spin lattices. Here we report systematic heat transport measurements on a honeycomb-lattice compound $BaCo_2(AsO_4)_2$, which manifests magnetic order in zero field. In a narrow in-plane field range after the magnetic order is nearly suppressed, in both perpendicular and parallel to the zigzag direction, a finite residual linear term of thermal conductivity is clearly observed, which is attributed to mobile fermionic excitations. In addition, the spin-phonon scattering rate exhibits a T-linear behavior when the order disappears. These observations suggest a partial QSL state with gapless spinon excitations in $BaCo_2(AsO_4)_2$, that emerges when a portion of the spins remains ordered, and vanishes as the spins become progressively polarized.

DOI: 10.1088/0256-307X/42/6/067304 CSTR: 32039.14.0256-307X.42.6.067304

Quantum spin liquids (QSLs) are novel highly entangled quantum phases of matter which host fractionalized excitations.[1–3] In contrast to conventional ordered magnets, QSLs are characterized by the absence of long-range magnetic order and spontaneous symmetry breaking down to absolute zero temperature. Frustrations are thought to play a significant role in inducing quantum fluctuation and stabilizing a QSL state.[1–3] Many geometrically frustrated systems have been considered as potential QSL candidates, such as prominent triangular-lattice compounds κ-(BEDT-TTF)$_2$Cu$_2$(CN)$_3$,[4–6] EtMe$_3$Sb[Pd(dmit)$_2$]$_2$,[7,8] $YbMgGaO_4$,[9–11] $NaYbSe_2$,[12] kagome-lattice $ZnCu_3(OH)_6Cl_2$,[13] and pyrochlore-lattice $Tb_2Ti_2O_7$, $Pr_2Zr_2O_7$, $Yb_2Ti_2O_7$, $Ce_2Zr_2O_7$, $Ce_2Sn_2O_7$.[14–17] On the other hand, Kitaev proposed a two-dimensional honeycomb-lattice model in 2006, in which frustrations originate from the bond-dependent Ising-type interactions.[18] The exactly solvable Kitaev model hosts localized Z_2 gauge fluxes and itinerant Majorana fermions, the ground state of which could be three gapped QSL states (A phases) or one gapless QSL state (B phase), depending on the magnitude relationship among the three nearest-neighbor anisotropic interactions of each site.[18] Intriguingly, by introducing a magnetic field, the B phase will convert into a gapped non-Abelian phase with anyon excitations obeying non-trivial braiding statistics, which could be utilized to realize intrinsically fault-tolerant topological quantum computations.[19,20]

In the pursuit of Kitaev QSL in real materials, transition metal compounds with partially filled $4d$ or $5d$ shells were proposed as promising candidates due to the intricate interplay between electronic correlation and spin-orbit coupling (SOC).[21] With strong SOC, the spatially anisotropic and bond-directional orbitals naturally lead to the Ising-type Kitaev interactions.[22] Following this reasoning, numerous studies have focused on Mott insulators of d^5 ions (exhibiting a t_{2g}^5 electronic configuration with pseudospin-1/2 Kramers doublet) with honeycomb lattice, including α-A_2IrO_3 (A = Li, Na, Cu), $A_3LiIr_2O_6$ (A = H, Ag, Cu) and α-$RuCl_3$.[23] Nevertheless, except for $H_3LiIr_2O_6$, these materials all present long-range magnetic order at low temperature because of inevitable perturbations, such as conventional Heisenberg interactions J resulting from direct d-d hybridization, off-diagonal symmetric anisotropy $\mathit{\Gamma}$ originating from both d-d and anion mediated d-p electron transfer and additional $\mathit{\Gamma}'$ term due to trigonal distortion of ligand octahedra in real materials.[24] Applying an external tuning parameter such as magnetic field is an effective way to suppress non-Kitaev terms, thereby approaching the Kitaev QSL state.[25,26] Therefore, finding materials with dominant Kitaev interaction and negligible non-Kitaev terms is crucial in the search of Kitaev QSL.

Recent theoretical studies have proposed that $3d^7$ Co^{2+} ions with honeycomb lattice is another potential platform to host Kitaev QSL.[27–30] In an octahedral crystal field environment, Co^{2+} ions form a $t_{2g}^5e_g^2$ electronic configuration with a high spin state ($S = 3/2$, $L = 1$), re-

[†] These authors contributed equally to this work.
[*] Corresponding author. Email: shiyan_li@fudan.edu.cn

sulting in a pseudospin-1/2 ground state Kramers doublet via SOC. Compared with weakly localized $4d$ and $5d$ systems, $3d$ systems possess more compact d orbitals, namely smaller long-range Heisenberg couplings. Furthermore, in spite of relatively weak SOC, the orbital moments remain active[29,30] and the additional e_g orbitals-related exchange processes are ferromagnetic, which compensate the antiferromagnetic Heisenberg interactions from t_{2g} orbitals and finally contribute to a dominant Kitaev coupling.[27,28] Experimentally, several cobaltates have been synthesized and investigated, such as $BaCo_2(PO_4)_2$,[31,32] $BaCo_2(AsO_4)_2$ (BCAO),[33–35] $Na_2Co_2TeO_6$[36–38] and $Na_3Co_2SbO_6$.[39–41] Although these materials all undergo a magnetic transition at low temperature, interestingly, BCAO was proposed to host an intermediate QSL regime by recent thermodynamic[34] and THz spectroscopy studies.[35]

In this Letter, with the motivation to identify QSL state in BCAO, we performed ultralow-temperature thermal conductivity measurements—a powerful technique for detecting low-energy quasiparticles—on high-quality BCAO single crystals down to 80 mK under in-plane magnetic fields. When the magnetic order is nearly suppressed by a weak field of $\mu_0 H \sim 0.5$ T, a finite residual linear term κ_0/T shows up, which demonstrates the existence of mobile fractionalized spinon excitations. This spinon contribution of κ_0/T persists in a narrow field range in both field directions (perpendicular and parallel to the zigzag direction), before the spins are more and more polarized. In addition, in the intermediate regime, finite spin-phonon scattering rates are observed in the zero-temperature limit, reinforcing the presence of gapless spin excitations. More interestingly, the spin-phonon scattering rate satisfies a T-linear dependence when the magnetic order disappears. These results imply a partial QSL state with gapless spinon excitations in BCAO, that emerges when a portion of the spins remains ordered, and vanishes as the spins become progressively polarized.

Magnetic Phase Diagram. The crystal of BCAO is sketched in Fig. 1(a), edge-sharing CoO_6 octahedra form a two-dimensional (2D) layered honeycomb lattice which is stacked along c axis with an ABC periodicity. Here, K_x, K_y and K_z denote the bond-dependent Kitaev interactions between the nearest-neighborhood Co^{2+} ions. The crystallographic a axis is along the zigzag chain while b axis is along the armchair direction, corresponding to the $[11\bar{2}]$ and $[\bar{1}10]$ directions in the (x, y, z) spin-axis coordinate, respectively. The Curie-Weiss temperature of BCAO is $\Theta_c = -167.7$ K and $\Theta_{ab} = 33.8$ K, respectively, indicating interplane antiferromagnetic and in-plane ferromagnetic exchange couplings,[34] like α-$RuCl_3$. Unlike α-$RuCl_3$, no stacking faults or structural domains are detected in BCAO.

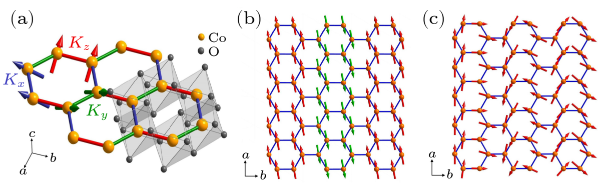

Fig. 1. Crystal structure and spin configuration of $BaCo_2(AsO_4)_2$. (a) Crystal structure of $BaCo_2(AsO_4)_2$ in ab plane and definitions of crystallographic axes a, b, c as well as the spin axes x, y, z. Spin x, y, z axes, perpendicular to Co-Co bond, are determined by bond-dependent Kitaev interactions K_x, K_y and K_z. Yellow and gray circles represent Co^{2+} and O^{2-}, respectively. (b) Double zigzag spin-chains form a ↑↑↓↓ pattern with small out-of-plane canting angle. (c) In-plane helical structure of spin spiral state, showing the stacking of weakly coupled quasi-ferromagnetic chains.[33]

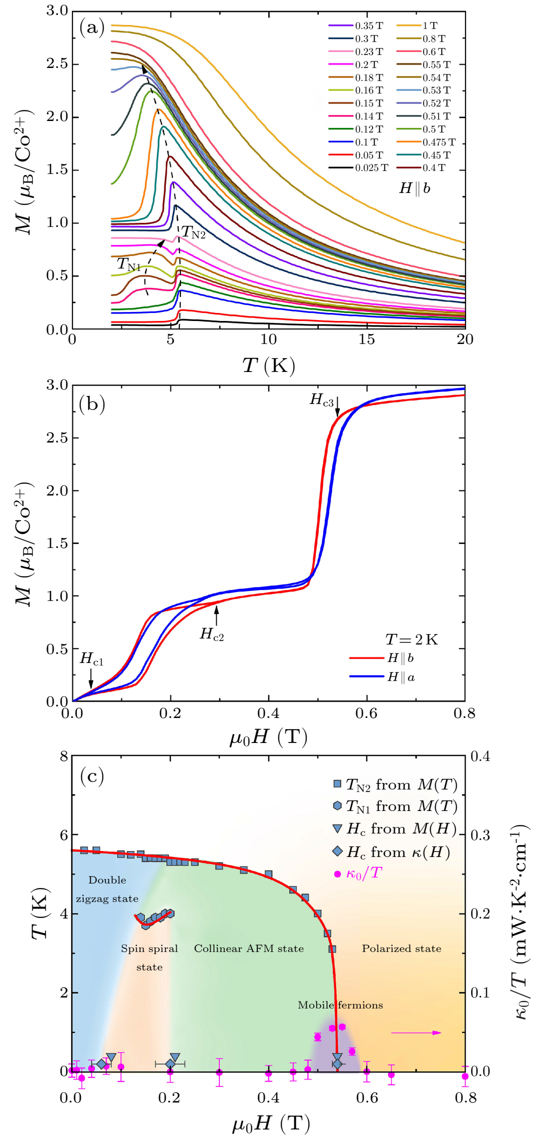

Fig. 2. In-plane field manipulation of the magnetic structure and the phase diagram for $H \parallel b$. (a) Temperature-dependent magnetic susceptibilities of $BaCo_2(AsO_4)_2$. The dashed arrows indicate two phase transitions at T_{N1} and T_{N2} for $H \parallel b$. (b) Field-dependent magnetization for fields along both a and b axes at 2 K, showing small in-plane anisotropy. The critical fields are labeled as H_{c1}, H_{c2} and H_{c3} with black arrows. (c) The obtained phase diagram for $H \parallel b$, exhibiting the evolution between several magnetic ordered states, intermediate regime, and polarized state, respectively. The Néel temperatures T_{N1} and T_{N2} are determined from magnetization measurements in (a). The critical fields at 0.4 K are extracted from $M(H)$ curve in Fig. S2 and from $\kappa(H)$ curve at 0.2 K in Fig. 3(h). The magenta circles represent residual linear terms κ_0/T in thermal conductivity measurements from Fig. 4(d), constructing an intermediate regime where finite κ_0/T, namely, mobile gapless fermionic excitations emerge.

Figure 2(a) plots the magnetization from 2 to 20 K of BCAO in various magnetic fields parallel to b axis. A clear peak due to antiferromagnetic (AFM) transition is observed at $T_{\rm N2} = 5.4$ K at zero field and it gradually shifts towards lower temperature and eventually vanishes at about 0.54 T. Moreover, the magnetizations display a board hump $T_{\rm N1}$ within the magnetic field range of 0.13 to 0.21 T. The lower and upper bounds remain visible down to 0.4 K manifested by the steep drop/rise in the M-H curve (see Supplementary Note 2), indicating two successive metamagnetic transitions and realignments of in-plane spins. The first transition is from the double zigzag state to spin spiral state, the magnetic structures of which are illustrated in Figs. 1(b) and 1(c).[33] The spin spiral state presents weak ferromagnetic correlation, evidenced by the hysteresis loop in Fig. 2(b). With field increasing, the system will then undergo a second transition into the collinear AFM state, corresponding to the nearly 1/3 plateau of the saturated magnetization, as shown in Fig. 2(b). As a comparison, the magnetization in fields along a axis was also measured (see Supplementary Note 2), which illustrates weak in-plane anisotropy except that the polarization field is slightly higher in the a axis case.

The magnetic phase diagram summarized in Fig. 2(c) is roughly consistent with the previous report.[34] The phase boundaries below 0.7 K are mainly determined from our thermal conductivity measurements, which will be discussed later. Most importantly, in this work we will demonstrate that there may exist a gapless QSL regime after the AFM order is nearly suppressed, characterized by the finite residual linear term of thermal conductivity.

Field Dependence of Thermal Conductivity. The in-plane ultralow-temperature thermal conductivity of BCAO Sample A in zero and finite magnetic fields up to 8 T is displayed in Figs. 3(a)–3(e). The heat current is along a axis while the field is along b axis, as shown in the inset of Fig. 3(a). Figures 3(g) and 3(h) plot the field dependence of κ/T at several temperatures, and these isotherms exhibit almost the same behavior. As the magnetic field increases, κ/T first drops slightly until $\mu_0 H \sim 0.05$ T, then increases sharply for $\mu_0 H < 0.2$ T, followed by a second decrease until $\mu_0 H \sim 0.54$ T, then rises monotonously and finally saturates for $\mu_0 H > 5$ T. The critical fields are consistent with our magnetization results and the whole evolution trend is in accord with previous thermal conductivity results in the temperature range of 4 to 4.8 K.[34]

To explain the evolution of $\kappa(H)$ in BCAO, firstly we should underline that $\kappa(5\,{\rm T})$ and $\kappa(8\,{\rm T})$ are entirely due to phonons without being scattered by the magnetic system, since it saturates and reaches the boundary-limited value (see Supplementary Note 4). Thus, $\kappa(H)$ in lower fields are dominated by phonon thermal conductivity scattered by other possible field-dependent scatters such as magnetic impurities and spin excitations (spinons, magnons). However, with increasing field, the scattering of phonons by magnetic impurities will weaken due to the growth of Zeeman gap, which cannot satisfy the whole complicated evolution of $\kappa(H)$ and cannot be the chief culprit. Hence, the inelastic scattering of phonons by spin excitations plays a significant role in determining $\kappa(H)$.

In general, the anomalies of $\kappa(H)$ are related to field-induced magnetic transitions as well as the variation in the strength of phonons scattering in frustrated spin systems. Owing to the spin fluctuations near critical magnetic field, κ will typically reach a local minimum in the vicinity, such as the observed two minima at $H_{\rm c1}$ and $H_{\rm c3}$ in Fig. 3(h). Among them, the least value of κ, located at $H_{\rm c3}$ ($\sim$0.54 T), corresponds to the end of the magnetic order. The prior two extreme points at $H_{\rm c1}$ ($\sim$0.05 T) and $H_{\rm c2}$ ($\sim$0.2 T) clearly marks the boundaries of the spin spiral state. It is elusive that κ exhibits a maximum at $H_{\rm c2}$ instead, which may mean that the two adjacent ordered states have close energy. Even so, the shape of $\kappa(H)$ is roughly in accord with the evolution of field-induced magnon gap detected by recent THz and INS measurements,[35,42]

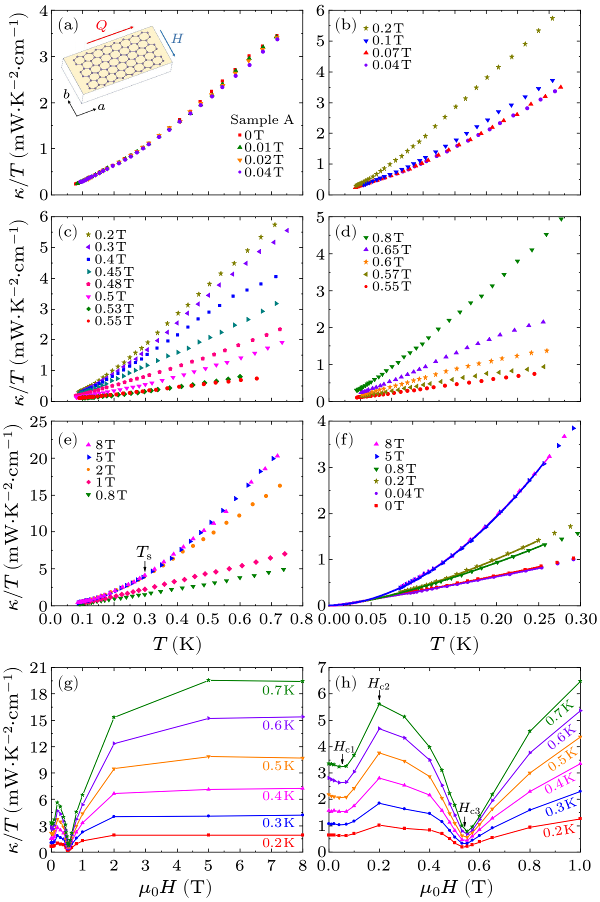

Fig. 3. Heat transport results of $BaCo_2(AsO_4)_2$ Sample A at various applied fields between (a) 0–0.04 T, (b) 0.04–0.2 T, (c) 0.2–0.55 T, (d) 0.55–0.8 T, and (e) 0.8–8 T. The inset in (a) shows the configuration of $Q \parallel a$ and $H \parallel b$, here Q represents the heat current. An overlap region in (e) is clearly shown below the temperature $T_{\rm s}$ marked by a black arrow, above which a bifurcation happens. (f) Thermal conductivity for several fields in magnetic ordered states and polarized state, plotted as κ/T versus T. The solid lines represent fittings to $\kappa/T = a + bT^{\alpha-1}$ below 0.25 K. The values of κ_0/T are negligible for these fields. (g) and (h) Field dependence of thermal conductivity plotted within two field ranges. The anomalies are labeled as $H_{\rm c1}$, $H_{\rm c2}$, and $H_{\rm c3}$ with black arrows, which indicate several magnetic phase transitions.

suggesting the modulation by spin-phonon scattering. In the spin spiral state, owing to the weak ferromagnetic correlation, the magnons are increasingly gapped out,[42] which weakens the spin-phonon scattering and leads to the enhancement of κ. In the polarized state above H_{c3}, the suppression of spin-phonon scattering, due to the alignment of spins (growth of magnon gap) with increasing magnetic field, results in the monotonical increase of κ. Such a magnon gap mediated phonon thermal conductivity is similar to $MnBi_2Te_4$.[43]

In fact, note that $\kappa(2\,T)$ almost overlaps with $\kappa(8\,T)$ below about 0.3 K, above which a bifurcation deviated from pure phonon contribution happens, as shown in Fig. 3(e), indicating additional phonon scattering by magnetic excitations emerging from a small gap. The presence of a small population of thermally excited low-energy magnetic excitations out of the gap in the polarized state can explain the higher saturated field in thermal conductivity than that in dc magnetization. The case for specific heat is the same as that for thermal conductivity (see Supplementary Note 3). Below we focus on the residual linear term of thermal conductivity in different states.

Absence of Residual Linear Term κ_0/T in Magnetically Ordered States and Spin Polarized State. In Fig. 3(f), we fitted the thermal conductivity data below 0.25 K for $\mu_0 H = 0$, 0.04, 0.2, 0.8, 5, and 8 T to $\kappa/T = a + bT^{\alpha-1}$, where aT and bT^{α} represent contributions from itinerant fermionic excitations κ_s and phonons $\kappa_{ph}(T, H)$, respectively.[44,45] For phonons, the power α equals 3 at the boundary scattering limit and will typically be reduced to between 2 and 3 due to the specular reflections at the sample surfaces.[44,45] Note that the power will usually further weaken when considering spin-phonon scattering in spin systems, nevertheless, it will not blur the validity of extracting positive residual linear term (see Supplementary Note 5 for more details of the fitting results). Furthermore, if gapless AFM spin waves (magnons) exist, their contributions behave as T^3 and will not obstruct our analysis as well.[46] The fitting yields $\kappa_0/T \equiv a = 0.002 \pm 0.008\,\mathrm{mW{\cdot}K^{-2}{\cdot}cm^{-1}}$ for 0 T, $0.004 \pm 0.011\,\mathrm{mW{\cdot}K^{-2}{\cdot}cm^{-1}}$ for 0.04 T, $-0.001 \pm 0.013\,\mathrm{mW{\cdot}K^{-2}{\cdot}cm^{-1}}$ for 0.2 T, $-0.006 \pm 0.013\,\mathrm{mW{\cdot}K^{-2}{\cdot}cm^{-1}}$ for 0.8 T, $0.009 \pm 0.013\,\mathrm{mW{\cdot}K^{-2}{\cdot}cm^{-1}}$ for 5 T, and $\kappa_0/T = -0.001 \pm 0.012\,\mathrm{mW{\cdot}K^{-2}{\cdot}cm^{-1}}$ for 8 T, respectively. Considering the typical error bar $\pm 0.005\,\mathrm{mW{\cdot}K^{-2}{\cdot}cm^{-1}}$ caused by our experimental setup and principle, the κ_0/T of BCAO at these magnetic fields are virtually zero, which is reasonable in these magnetically ordered states and spin polarized state. Our primary focus is whether κ_0/T emerges in the intermediate regime when the magnetic order is nearly suppressed.

Mobile Gapless Fermionic Excitations in the Intermediate Regime. In Fig. 4(a), we fitted the data below 0.25 K to $\kappa/T = a + bT^{\alpha-1}$ for magnetic fields from 0.4 T to 0.65 T. Although the fittings give $\kappa_0/T \equiv a \approx 0$ for $\mu_0 H = 0.4$, 0.45, 0.48, 0.6, and 0.65 T, strikingly, finite κ_0/T is obtained for the fields between 0.48 and 0.6 T. To see more details, we plot the thermal conductivity data for $\mu_0 H = 0.5$, 0.53, 0.55 and 0.57 T with error bar in Fig. 4(b).

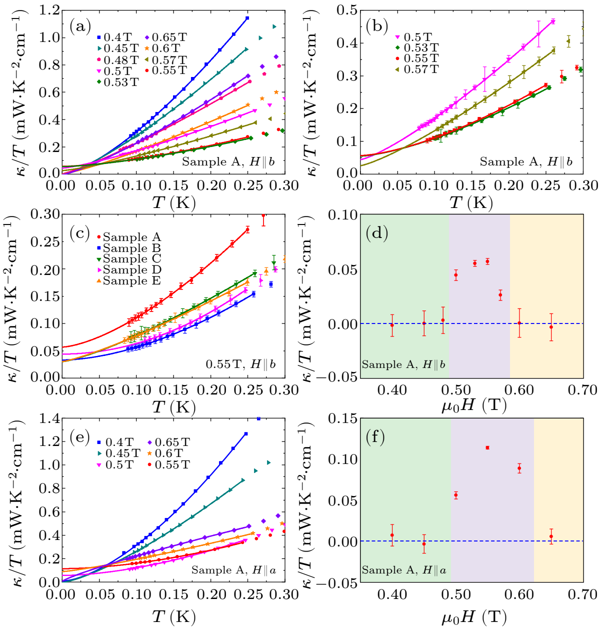

Fig. 4. Heat transport results in the vicinity of the intermediate regime of $BaCo_2(AsO_4)_2$ Sample A. (a) Thermal conductivity data under magnetic fields from 0.4 to 0.55 T for $H \parallel b$. The solid lines represent fittings below 0.25 K, the same as in Fig. 3. The data with finite residual linear terms are replotted in (b). (c) Thermal conductivity of five different samples at 0.55 T. All the data yield finite residual linear terms, manifesting the highly reproducibility of our results. (d) Field dependence of κ_0/T. The finite κ_0/T exists within the field range from about 0.5 to 0.6 T, which outlines the boundary of partial gapless QSL state. (e) Thermal conductivity results for $H \parallel a$. Finite κ_0/T is observed at several fields illustrated in (f), identifying that the partial gapless QSL state persists under magnetic fields along both a and b axes.

The fittings give $\kappa_0/T = 0.044 \pm 0.005\,\mathrm{mW{\cdot}K^{-2}{\cdot}cm^{-1}}$, $0.055 \pm 0.003\,\mathrm{mW{\cdot}K^{-2}{\cdot}cm^{-1}}$, $0.057 \pm 0.003\,\mathrm{mW{\cdot}K^{-2}{\cdot}cm^{-1}}$, and $0.026 \pm 0.005\,\mathrm{mW{\cdot}K^{-2}{\cdot}cm^{-1}}$, respectively.

To confirm reproducibility, we performed thermal conductivity measurements on four more samples and the data at 0.55 T are plotted in Fig. 4(c). The fittings yield $\kappa_0/T = 0.033 \pm 0.001\,\mathrm{mW{\cdot}K^{-2}{\cdot}cm^{-1}}$ for Sample B, $0.030 \pm 0.003\,\mathrm{mW{\cdot}K^{-2}{\cdot}cm^{-1}}$ for Sample C, $0.044 \pm 0.001\,\mathrm{mW{\cdot}K^{-2}{\cdot}cm^{-1}}$ for sample D, and $0.030 \pm 0.002\,\mathrm{mW{\cdot}K^{-2}{\cdot}cm^{-1}}$ for sample E, which shows that our results are highly reproducible.

These finite κ_0/T immediately reveal mobile gapless fermionic excitations in BCAO, which is reminiscent of a quantum spin liquid state. Indeed, the T-linear behavior in κ_{xx} in the zero-temperature limit has been theoretically predicted by itinerant Majorana fermions on the honeycomb lattice.[47] According to the method in Ref. [7], assuming the fermionic excitations are analogous to electrons near the Fermi surface in metals, and with linear dispersion relation, the mean free path (l_s) can be estimated by calculating $\frac{\kappa_0}{T} = \frac{\pi k_B^2}{9\hbar} \frac{l_s}{a' d} = \frac{\pi}{9} (\frac{k_B}{\hbar})^2 \frac{J}{d} \tau_s$. Here $a' = a/\sqrt{3} = 2.89\,\text{Å}$ and $d \approx c/3 = 7.83\,\text{Å}$ represent the nearest-neighbor in-plane and out-of-plane Co-Co distance in BCAO, respectively.[34] From the observed $\kappa_0/T = 0.057\,\mathrm{mW{\cdot}K^{-2}{\cdot}cm^{-1}}$ for $\mu_0 H = 0.55\,T$, the obtained l_s is 128.4 Å, indicating that the fermionic excitations are mobile to about 44 times the in-plane interspin distance without being scattered.

For comparison, the thermal conductivity of Sample A with field along a axis is also measured, as plotted in Fig. 4(e). Similar fits below 0.25 K yield $\kappa_0/T = 0.056 \pm 0.004\,\mathrm{mW{\cdot}K^{-2}{\cdot}cm^{-1}}$ for 0.5 T, $0.114 \pm 0.002\,\mathrm{mW{\cdot}K^{-2}{\cdot}cm^{-1}}$ for 0.55 T, $0.089 \pm 0.006\,\mathrm{mW{\cdot}K^{-2}{\cdot}cm^{-1}}$ for 0.6 T, respectively. Thus, a finite κ_0/T is observed in both field directions. Interestingly, the fitting gives $\kappa_0/T = 0.005 \pm 0.009\,\mathrm{mW{\cdot}K^{-2}{\cdot}cm^{-1}}$ with $\alpha = 1.84 \pm 0.02$ for 0.65 T. The power is abnormally slightly lower than 2, similar to observations in various other QSL candidates, such as $YbMgGaO_4$,[11] $EtMe_3Sb[Pd(dmit)_2]_2$,[48,49] $ZnCu_3(OH)_6Cl_2$[50] and $NaYbSe_2$,[51] and this sublinear behavior usually arises from strong spin-phonon scattering.

The field dependences of κ_0/T in two field directions are summarized in Figs. 4(d) and 4(f). More detailed data of different samples can be seen in the Supplementary Note 6. On the whole, the field range of gapless QSL state is relatively wider for $H \parallel a$, which may link to the slightly higher polarization field along a axis. Note that the QSL regime has some overlaps with collinear AFM state and partially polarized state, as sketched in the phase diagram of Fig. 2(d). Thus, we here conceive a possible scenario of coexistence of the gapless QSL state with a partially AFM ordered state (left of H_{c3}) and a partially polarized state (right of H_{c3}) . In such a partial QSL state, strong quantum fluctuations in the vicinity of H_{c3} lead to the formation of a portion of disordered spins, which contribute to fractionalized spinon excitations. A pure QSL state may exist at exactly the critical field H_{c3} when the magnetic order disappears and before the spins are polarized. Further studies, such as μSR and NMR/NQR, are warranted to verify this scenario.

T-Linear Spin-Phonon Scattering Rate in the Intermediate Regime. To gain more information about the spin-phonon scattering in BCAO, we now seek to quantify the scattering rate, following the method in Refs. [52–54]. According to Matthiessen's rule, the total scattering rate is the sum of all independent origins, $\tau^{-1} = \tau_{\mathrm{p}}^{-1} + \tau_{\mathrm{sp}}^{-1}$, where τ_{p} and τ_{sp} represent the intrinsic phononic and additional spin-phonon scattering relaxation times, respectively. Since κ saturates beyond 5 T and reaches the boundary scattering value (see Supplementary Note 4), the thermal conductivity data at highest field can be regarded as pure phonon contribution κ_{ph} without spin-phonon scattering (due to the large magnon gap in the spin-polarized state). Thus, combining with the kinetic formula $\kappa_{\mathrm{ph}}(T,H) = \frac{1}{3}C_{\mathrm{ph}}v_{\mathrm{ph}}l_{\mathrm{ph}}(T,H) = \frac{1}{3}C_{\mathrm{ph}}v_{\mathrm{ph}}^2\tau(T,H)$, the ratio $\tau_{\mathrm{p}}/\tau_{\mathrm{sp}}$ is expressed as $\kappa_{\mathrm{ph}}/\kappa_{\mathrm{ph}}(T,H) - 1$ and plotted in Fig. 5.

In the magnetically ordered state below H_{c3}, the temperature dependence of scattering rate shows a thermal-excited Arrhenius-type behavior, which is compatible with the phenomenon that phonon is scattered by low-energy thermally-excited magnons out of a gap. Though we do not unveil a universal function to capture all the data, the more and more bulging shape of the curves beyond 0.2 T in Fig. 5(a) suggests the gradual decrease of the gap,

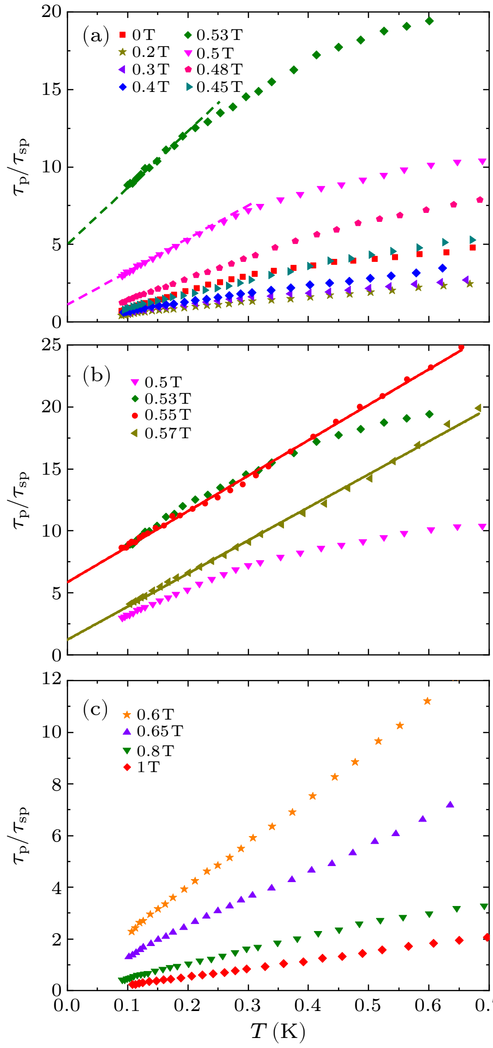

Fig. 5. Spin-phonon scattering rate of $BaCo_2(AsO_4)_2$ Sample A for $H \parallel b$. Temperature dependence of $\tau_{\mathrm{p}}/\tau_{\mathrm{sp}}$ at different field regions in (a) the magnetically ordered state, (b) the partial QSL state, and (c) the polarized state. The dashed lines mean linear extrapolations to absolute zero temperature and point to finite intercepts. The solid lines represent linear fittings with positive intercepts, which indicate gapless fermionic excitations.

presuming an exponential form $\sim \mathrm{e}^{-\Delta/k_{\mathrm{B}}T}$. This behavior is consistent with the evolution of the magnon gap detected in the THz and INS experiments.[35,42] Interestingly, in contrast to other curves, the linear extrapolation to absolute zero temperature for 0.5 T and 0.53 T point to positive intercepts, which mean finite spin-phonon scattering rates, in other words, finite density of states of gapless spin excitations.

The cases for 0.55 T and 0.57 T are the same, and more strikingly, the ratio $\tau_{\mathrm{p}}/\tau_{\mathrm{sp}}$ obeys a T-linear dependence with positive intercepts for the whole temperature range from 0.1 to 0.7 K, as plotted in Fig. 5(b). Since the pure phonon thermal conductivity at 8 T is dominated by boundary scattering, τ_{p} is weakly temperature dependent at low temperature (see Supplementary Note 4). Hence, the deduced spin-phonon scattering rate τ_{sp}^{-1} is proportional to T, which is reminiscent of the electron-phonon scattering $\tau_{\mathrm{ep}}^{-1} \sim T$,[55,56] implying the fermionic nature of the gapless spin excitations. Note that a recent thermal conductivity study on triangular-lattice QSL candidate $PrMgAl_{11}O_{19}$ identifies the spin-phonon scattering rate $\tau_{sp}^{-1} \sim T e^{-\Delta/k_B T}$, in which a T-linear prefactor has also been observed. [54]

Hence, the analysis of spin-phonon scattering rate reinforces the emergence of gapless spinons in the intermediate regime, and the field evolution of τ_p/τ_{sp} is consistent with our scenario of a coexistence of the gapless QSL state with partially AFM ordered state. Beyond 0.5 T, the spin excitations are composed of dominant thermally-excited magnons out of a small gap and gapless spinons which are contributed by the gradually disordered portion of spins. The magnetic order vanishes around 0.55 T, and the only scatters are gapless spinons, thus leading to the abrupt alternation of the temperature dependence of spin-phonon scattering rate as well as the abnormal peak-like feature of phonon power α (see Supplementary Note 5).

Above 0.6 T, the extrapolated intercepts fade away and the curves start to bend, as shown in Fig. 5(c), indicating the disappearance of gapless spinons and the gradual increase of magnon gap in the polarized state, which is consistent with a recent thermal conductivity study above 0.49 K of the polarized state. [57]

Discussion. In the search of quantum spin liquids, detecting the emergent fractionalized spinon excitations is crucial and ultralow-temperature thermal conductivity measurement is one of the most low-energy experimental techniques. [58] Previously triangular-lattice organic compound $EtMe_3Sb[Pd(dmit)_2]_2$ [7] has been reported to exhibit a huge κ_0/T of $2\,mW{\cdot}K^{-2}{\cdot}cm^{-1}$, however, it cannot be reproduced by other groups. [48,49] To our knowledge, there is still no reproducible report of the existence of finite κ_0/T in any QSL candidate so far, including honeycomb-lattice Kitaev materials such as α-$RuCl_3$, [59,60] $Na_2Co_2TeO_6$ [61,62] and $Na_3Co_2SbO_6$. [63] For $Na_2Co_2TeO_6$, a nonzero $\kappa_0/T = 0.038\,mW{\cdot}K^{-2}{\cdot}cm^{-1}$ was initially reported at 0 T, termed as a fractionalized antiferromagnetic state, while no κ_0/T was observed when the magnetic order is suppressed. [61] However, at first glance, the conclusion is strange since it directly violates the definition of QSL. In fact, a recent thermal conductivity measurement by another group has revealed an upturn at lower temperature, which causes the misjudgment about κ_0/T. [62] Since no such upturn is observed in our BCAO samples down to 80 mK, it is striking that a finite κ_0/T is observed in a narrow field range when magnetic order is nearly suppressed. This is highly reproducible, in several samples and two field directions. Below we discuss the possible underlying physics to form this exotic gapless QSL state.

Firstly, we should emphasize that our results are in sharp contrast to the gapless Kitaev spin liquid with a static Z_2 guage field (B phase). Within the framework of pure Kitaev model, the itinerant Majorana fermions are gapless with two Dirac nodes. [18] When applying a magnetic field, B phase will acquire a gap $\Delta_M \sim h_x h_y h_z/K^2$ (here, h_i represents the Cartesian component of the applied field) in the bulk and thus form a topologically protected gapless chiral Majorana edge mode. [18] Therefore, it is obvious that the bulk excitations remain gapless if at least one component disappears. Due to the particular geometry and oxygen-mediated hopping of edge-shared CoO_6 octahedra in BCAO, which are similar to iridates, [22] the above condition can be realized when the magnetic field is applied along b axis, as depicted in Fig. 1(a). In other words, the Majorana gap has six-fold symmetry with respect to the in-plane magnetic field. This in-plane field-angle dependence of physical quantities has been observed in α-$RuCl_3$ by magnetization, [64] thermal Hall conductivity, [65] and specific heat [66] measurements. However, our results on thermal conductivity reveal the existence of gapless fermionic excitations when the fields are applied in both a and b axes for BCAO, which is apparently beyond the hypothesis.

Another possible scenario is that the intermediate regime is in line with a gapless U(1) quantum spin liquid with neutral spinon Fermi surfaces. [67,68] In this framework, the bulk gapless fermionic excitations will immediately open a gap when a magnetic field is applied, and then the system will undergo a quantum transition from the gapped Z_2 Kitaev QSL with non-Abelian Ising topological order to the intermediate gapless U(1) QSL as the field increases, and finally enter into a gapped trivial polarized state. [67] Especially, the gapless QSL state is stable even in the presence of additional small Heisenberg and off-diagonal gamma interactions. [67] This picture can be depicted by the analogy of fermiology of spinons. The gapped non-Abelian phase corresponds to a $p_x + ip_y$ chiral topological superconductor of fermionic spinons. Hence, applying a magnetic field will destroy the superconducting order and form a spinon metal with a gapless Fermi surface coupled to a massless U(1) gauge field. [67] Theoretically, considering the inevitable disorder of real samples, the gapless U(1) QSL system will exhibit a T-linear behavior in the in-plane thermal conductivity at the ultralow-temperature limit. [69] The prediction is consistent with our experimental observations. However, this scenario is based on dominate AFM Kitaev interaction, while the gapless QSL state is absent in the ferromagnetic case, [67,68] which cannot reconcile with BCAO. Furthermore, the intermediate state has also been proposed unstable [70] or even nonexistent [71] when magnetic field is applied along b axis in honeycomb lattice. These disagreements with our observation of robust κ_0/T imply that more experimental and theoretical efforts are needed to determine the physical origin of the exotic gapless QSL state in BCAO. Interestingly, we notice that recent study demonstrated a novel mechanism to induce Majorana Fermi surfaces with U(1) degrees of freedom, independent of the sign of Kitaev interaction. [72]

Finally, we cannot exclude the scenario that BCAO is described by XXZ-J_1-J_3 model rather than extended Kitaev model ($JK\Gamma\Gamma'$). Indeed, whether there exists large Kitaev coupling in Co-based layered honeycomb system is still under debate. Recent theoretical studies [73–76] and INS experiments [42] have favored that third nearest neighbor Heisenberg interaction J_3 plays a significant role in $3d^7$ cobaltates, leading to dominant FM Heisenberg hopping with negligible Kitaev coupling in BCAO, similar to

$BaCo_2(PO_4)_2$.[32] The XXZ-J_1-J_3 model might also account for the small anisotropy in magnetizations observed in BCAO for two in-plane field orientations. Within this framework, the competition between J_1 and J_3 is a feasible mechanism to induce exchange frustration, thus approaching the gapless QSL state.[42,77–79]

In summary, we have measured the ultralow-temperature thermal conductivity of honeycomb-lattice $BaCo_2(AsO_4)_2$ single crystals down to 80 mK with in-plane magnetic field up to 8 T. At finite temperatures, the field dependence of the thermal conductivity exhibits a series of extreme points, corresponding to successive metamagnetic transitions. In the zero-temperature limit, finite residual linear terms contributed by mobile gapless fermionic excitations are clearly observed in fields along both a and b axes, when the magnetic order is nearly suppressed. Moreover, the spin-phonon scattering rate exhibits a T-linear dependence when the magnetic order disappears. These observations imply a field-induced intermediate regime where gapless spinon excitations emerge, suggesting a partial QSL state formed by the disordered portion of spins. It coexists with partially AFM ordered state (at the left side of H_{c3}) and partially polarized state (at the right side of H_{c3}). These results exclude the possibility of gapless Kitaev QSL and put strong constraints on the theoretical description of $BaCo_2(AsO_4)_2$.

Acknowledgements. We thank Tao Wu, Yi Zhou, and Hong Yao for helpful discussions. We acknowledge Dr. Chao Zhang from Instrumentation and Service Center for Physical Sciences at Westlake University for the assistance in low-temperature dc magnetization data acquisition. This research was funded by the National Natural Science Foundations of China (Grant Nos. 12034004 and 12174064), the Shanghai Municipal Science and Technology Major Project (Grant No. 2019SHZDZX01), and the Innovation Program for Quantum Science and Technology (Grant No. 2024ZD0300104). The single crystal growth and characterization efforts at Rice University are supported by U.S. DOE BES DE-SC0012311 and the Robert A. Welch Foundation under Grant No. C-1839, respectively (P.D.).

References

[1] Balents L 1973 *Nature* **464** 199
[2] Zhou Y, Kanoda K, and Ng T K 2017 *Rev. Mod. Phys.* **89** 025003
[3] Broholm C, Cava R J, Kivelson S A, Nocera D G, Norman M R, and Senthil T 2020 *Science* **367** eaay0668
[4] Shimizu Y, Miyagawa K, Kanoda K, Maesato M, and Saito G 2003 *Phys. Rev. Lett.* **91** 107001
[5] Yamashita S, Nakazawa Y, Oguni M, Oshima Y, Nojiri H, Shimizu Y, Miyagawa K, and Kanoda K 2008 *Nat. Phys.* **4** 459
[6] Yamashita M, Nakata N, Kasahara Y, Sasaki T, Yoneyama N, Kobayashi N, Fujimoto S, Shibauchi T, and Matsuda Y 2009 *Nat. Phys.* **5** 44
[7] Yamashita M, Nakata N, Senshu Y, Nagata M, Yamamoto H M, Kato R, Shibauchi T, and Matsuda Y 2010 *Science* **328** 1246
[8] Yamashita S, Yamamoto T, Nakazawa Y, Tamura M, and Kato R 2011 *Nat. Commun.* **2** 275
[9] Li Y S, Liao H J, Zhang Z, Li S Y, Jin F, Ling L S, Zhang L, Zou Y M, Pi L, Yang Z R, Wang J F, Wu Z H, and Zhang Q M 2015 *Sci. Rep.* **5** 16419
[10] Shen Y, Li Y D, Wo H L, Li Y S, Shen S D, Pan B Y, Wang Q S, Walker H C, Steffens P, Boehm M, Hao Y Q, Quintero-Castro D L, Harriger L W, Frontzek M D, Hao L J, Meng S Q, Zhang Q M, Chen G, and Zhao J 2016 *Nature* **540** 559
[11] Xu Y, Zhang J, Li Y S, Yu Y J, Hong X C, Zhang Q M, and Li S Y 2016 *Phys. Rev. Lett.* **117** 267202
[12] Dai P L, Zhang G N, Xie Y F, Duan C R, Gao Y H, Zhu Z H, Feng E X, Tao Z, Huang C L, Cao H B, Podlesnyak A, Granroth G E, Everett M S, Neuefeind J C, Voneshen D, Wang S, Tan G T, Morosan E, Wang X, Lin H Q, Shu L, Chen G, Guo Y F, Lu X Y, and Dai P C 2021 *Phys. Rev. X* **11** 021044
[13] Norman M R 2016 *Rev. Mod. Phys.* **88** 041002
[14] Gingras M J P and McClarty P A 2014 *Rep. Prog. Phys.* **77** 056501
[15] Gao B, Chen T, Tam D W, Huang C L, Sasmal K, Adroja D T, Ye F, Cao H B, Sala G, Stone M B, Baines C, Verezhak J A T, Hu H Y, Chung J H, Xu X H, Cheong S W, Nallaiyan M, Spagna S, Maple M B, Nevidomskyy A H, Morosan E, Chen G, and Dai P C 2019 *Nat. Phys.* **15** 1052
[16] Gaudet J, Smith E M, Dudemaine J, Beare J, Buhariwalla C R C, Butch N P, Stone M B, Kolesnikov A I, Xu G Y, Yahne D R, Ross K A, Marjerrison C A, Garrett J D, Luke G M, Bianchi A D, and Gaulin B D 2019 *Phys. Rev. Lett.* **122** 187201
[17] Sibille R, Gauthier N, Lhotel E, Porée V, Pomjakushin V, Ewings R A, Perring T G, Ollivier J, Wildes A, Ritter C, Hansen T C, Keen D A, Nilsen G J, Keller L, Petit S, and Fennell T 2020 *Nat. Phys.* **16** 546
[18] Kitaev A 2006 *Ann. Phys.* **31** 2
[19] Kitaev A Y 2003 *Ann. Phys.* **303** 2
[20] Nayak C, Simon S H, Stern A, Freedman M, and Sarma S D 2008 *Rev. Mod. Phys.* **80** 1083
[21] Witczak-Krempa W, Chen G, Kim Y B, and Balents L 2014 *Annu. Rev. Condens. Matter Phys.* **5** 57
[22] Jackeli G and Khaliullin G 2009 *Phys. Rev. Lett.* **102** 017205
[23] Takagi H, Takayama T, Jackeli G, Khaliullin G, and Nagler S E 2019 *Nat. Rev. Phys.* **1** 264
[24] Winter S M, Tsirlin A A, Daghofer M, van den Brink J, Singh Y, Gegenwart P, and Valentí R 2017 *J. Phys. Condens. Matter* **29** 493002
[25] Ruiz A, Frano A, Breznay N P, Kimchi I, Helm T, Oswald I, Chan J Y, Birgeneau R J, Islam Z, and Analytis J G 2017 *Nat. Commun.* **8** 961
[26] Sears J A, Zhao Y, Xu Z, Lynn J W, and Kim Y J 2017 *Phys. Rev. B* **95** 180411
[27] Liu H M and Khaliullin G 2018 *Phys. Rev. B* **97** 014407
[28] Sano R, Kato Y, and Motome Y 2018 *Phys. Rev. B* **97** 014408
[29] Liu H M, Chaloupka J, and Khaliullin G 2020 *Phys. Rev. Lett.* **125** 047201
[30] Samanta S, Detrattanawichai P, Na-Phattalung S, and Kim H S 2022 *Phys. Rev. B* **106** 195136
[31] Zhong R D, Chung M, Kong T, Nguyen L T, Lei S M, and Cava R J 2018 *Phys. Rev. B* **98** 220407
[32] Nair H S, Brown J M, Coldren E, Hester G, Gelfand M P, Podlesnyak A, Huang Q, and Ross K A 2018 *Phys. Rev. B* **97** 134409
[33] Regnault L P, Boullier C, and Lorenzo J E 2018 *Heliyon* **4** e00507
[34] Zhong R D, Gao T, Ong N P, and Cava R J 2020 *Sci. Adv.* **6** eaay6953
[35] Zhang X S, Xu Y Y, Halloran T, Zhong R D, Broholm C, Cava R J, Drichko N, and Armitage N P 2023 *Nat. Mater.* **22** 58

[36] Lefrançois E, Songvilay M, Robert J, Nataf G, Jordan E, Chaix L, Colin C V, Lejay P, Hadj-Azzem A, Ballou R, and Simonet V 2016 *Phys. Rev. B* **94** 214416
[37] Lin G T, Jeong J, Kim C, Wang Y, Huang Q, Masuda T, Asai S, Itoh S, Günther G, Russina M, Lu Z L, Sheng J M, Wang L, Wang J C, Wang G H, Ren Q Y, Xi C Y, Tong W, Ling L S, Liu Z X, Wu L S, Mei J W, Qu Z, Zhou H D, Wang X Q, Park J G, Wan Y, and Ma J 2021 *Nat. Commun.* **12** 5559
[38] Yao W L, Zhao Y, Qiu Y M, Balz C, Stewart J R, Lynn J W, and Li Y 2023 *Phys. Rev. Res.* **5** L022045
[39] Yan J Q, Okamoto S, Wu Y, Zheng Q, Zhou H D, Cao H B, and McGuire M A 2019 *Phys. Rev. Mater.* **3** 074405
[40] Vavilova E, Vasilchikova T, Vasiliev A, Mikhailova D, Nalbandyan V, Zvereva E, and Streltsov S V 2023 *Phys. Rev. B* **107** 054411
[41] Gu Y C, Jin X H, and Li Y 2025 *Chin. Phys. Lett.* **42** 027303
[42] Halloran T, Desrochers F, Zhang E Z, Chen T, Chern L E, Xu Z J, Winn B, Graves-Brook M, Stone M B, Kolesnikov A I, Qiu Y M, Zhong R D, Cava R, Kim Y B, and Broholm C 2023 *Proc. Natl. Acad. Sci. USA* **120** e2215509119
[43] Vu D D, Nelson R A, Wooten B L, Barker J, Goldberger J E, and Heremans J P 2023 *Phys. Rev. B* **108** 144402
[44] Sutherland M, Hawthorn D G, Hill R W, Ronning F, Wakimoto S, Zhang H, Proust C, Boaknin E, Lupien C, Taillefer L, Liang R X, Bonn D A, Hardy W N, Gagnon R, Hussey N E, Kimura T, Nohara M, and Takagi H 2003 *Phys. Rev. B* **67** 174520
[45] Li S Y, Bonnemaison J B, Payeur A, Fournier P, Wang C H, Chen X H, and Taillefer L 2008 *Phys. Rev. B* **77** 134501
[46] Li S Y, Taillefer L, Wang C H, and Chen X H 2005 *Phys. Rev. Lett.* **95** 156603
[47] Nasu J, Yoshitake J, and Motome Y 2017 *Phys. Rev. Lett.* **119** 127204
[48] Ni J M, Pan B L, Song B Q, Huang Y Y, Zeng J Y, Yu Y J, Cheng E J, Wang L S, Dai D Z, Kato R, and Li S Y 2019 *Phys. Rev. Lett.* **123** 247204
[49] Bourgeois-Hope P, Laliberté F, Lefrançois E, Grissonnanche G, de Cotret S R, Gordon R, Kitou S, Sawa H, Cui H, Kato R, Taillefer L, and Doiron-Leyraud N 2019 *Phys. Rev. X* **9** 041051
[50] Huang Y Y, Xu Y, Wang L, Zhao C C, Tu C P, Ni J M, Wang L S, Pan B L, Fu Y, Hao Z Y, Liu C, Mei J W, and Li S Y 2021 *Phys. Rev. Lett.* **127** 267202
[51] Zhu Z H, Pan B L, Nie L P, Ni J M, Yang Y X, Chen C S, Jiang C Y, Huang Y Y, Cheng E J, Yu Y J, Miao J J, Hillier A D, Chen X H, Wu T, Zhou Y, Li S Y, and Shu L 2023 *The Innovation* **4** 100459
[52] Hong X C, Behnami M, Yuan L, Li B Q, Brenig W, Büchner B, Li Y S, and Hess C 2022 *Phys. Rev. B* **106** L220406
[53] Barthélemy Q, Lefrançois É, Baglo J, Bourgeois-Hope P, Chatterjee D, Lefloïc P, Velázquez M, Balédent V, Bernu B, Doiron-Leyraud N, Bert F, Mendels P, and Taillefer L 2023 *Phys. Rev. B* **107** 054434
[54] Tu C P, Ma Z, Wang H R, Jiao Y H, Dai D Z, and Li S Y 2024 *Phys. Rev. Res.* **6** 043147
[55] Ziman J M 1956 *Philos. Mag.* **1** 191
[56] Butler W H and Williams R K 1978 *Phys. Rev. B* **18** 6483
[57] Hu J Y, Zhong R D, Czajka P, Gao T, Cava R J, and Ong N P 2024 arXiv:2408.00873 [cond-mat.str-el]
[58] Li N, Zhao X, and Sun X F 2024 *Chin. Phys. Lett.* **41** 127501
[59] Yu Y J, Xu Y, Ran K J, Ni J M, Huang Y Y, Wang J H, Wen J S, and Li S Y 2018 *Phys. Rev. Lett.* **120** 067202
[60] Suetsugu S, Ukai Y, Shimomura M, Kamimura M, Asaba T, Kasahara Y, Kurita N, Tanaka H, Shibauchi T, Nasu J, Motome Y, and Matsuda Y 2022 *J. Phys. Soc. Jpn.* **91** 124703
[61] Guang S K, Li N, Luo R L, Huang Q, Wang Y Y, Yue X Y, Xia K, Li Q J, Zhao X, Chen G, Zhou H D, and Sun X F 2023 *Phys. Rev. B* **107** 184423
[62] Hong X C, Gillig M, Yao W L, Janssen L, Kocsis V, Gass S, Li Y, Wolter A U B, Büchner B, and Hess C 2024 *npj Quantum Mater.* **9** 18
[63] Fan H R, Chen Y, Gu Y C, Li X T, Li Y, and Lin X 2025 *Phys. Rev. B* **111** 085119
[64] Balz C, Janssen L, Lampen-Kelley P, Banerjee A, Liu Y H, Yan J Q, Mandrus D G, Vojta M, and Nagler S E 2021 *Phys. Rev. B* **103** 174417
[65] Yokoi T, Ma S, Kasahara Y, Kasahara S, Shibauchi T, Kurita N, Tanaka H, Nasu J, Motome Y, Hickey C, Trebst S, and Matsuda Y 2021 *Science* **373** 568
[66] Tanaka O, Mizukami Y, Harasawa R, Hashimoto K, Hwang K, Kurita N, Tanaka H, Fujimoto S, Matsuda Y, Moon E G, and Shibauchi T 2022 *Nat. Phys.* **18** 429
[67] Hickey C and Trebst S 2019 *Nat. Commun.* **10** 530
[68] Kaib D A S, Winter S M, and Valentí R 2019 *Phys. Rev. B* **100** 144445
[69] Nave C P and Lee P A 2007 *Phys. Rev. B* **76** 235124
[70] Jiang Y F, Devereaux T P, and Jiang H C 2019 *Phys. Rev. B* **100** 165123
[71] Kim B H, Sota S, Shirakawa T, Yunoki S, and Son Y W 2020 *Phys. Rev. B* **102** 140402
[72] Takikawa D and Fujimoto S 2019 *Phys. Rev. B* **99** 224409
[73] Maksimov P A, Ushakov A V, Pchelkina Z V, Li Y, Winter S M, and Streltsov S V 2022 *Phys. Rev. B* **106** 165131
[74] Das S, Voleti S, Saha-Dasgupta T, and Paramekanti A 2021 *Phys. Rev. B* **104** 134425
[75] Winter S M 2022 *J. Phys. Mater.* **5** 045003
[76] Liu X Y and Kee H Y 2023 *Phys. Rev. B* **107** 054420
[77] Watanabe Y, Trebst S, and Hickey C 2022 arXiv:2212.14053 [cond-mat.str-el]
[78] Bose A, Routh M, Voleti S, Saha S K, Kumar M, Saha-Dasgupta T, and Paramekanti A 2023 *Phys Rev B* **108** 174422
[79] Bose A and Paramekanti A 2025 *Phys. Rev. B* **111** 104435